Published in final edited form as:
J Bone Miner Res. 2013 October ; 28(10): 2094–2108. doi:10.1002/jbmr.1962.

Disruption of LRP6 in osteoblasts blunts the bone anabolic activity of PTH

Changjun Li[1,2], **Qiujuan Xing**[1,3], **Bing Yu**[1], **Hui Xie**[1], **Weishan Wang**[2], **Chenhui Shi**[2], **Janet L. Crane**[1], **Xu Cao**[1], and **Mei Wan**[1,*]

[1]Department of Orthopaedic Surgery, Johns Hopkins University School of Medicine, Baltimore, MD 21205, USA

[2]Shihezi Medical Collage, Shihezi Univeristy, Xinjiang, China

[3]Longhua Hospital, Shanghai University of Traditional Chinese Medicine, Shanghai, China

Abstract

Mutations in Low-density lipoprotein receptor-related protein 6 (LRP6) are associated with human skeletal disorders. LRP6 is required for parathyroid hormone (PTH)-stimulated signaling pathways in osteoblasts. We investigated whether LRP6 in osteoblasts directly regulates bone remodeling and mediates the bone anabolic effects of PTH by specifically deleting LRP6 in mature osteoblasts in mice (LRP6 KO). Three month-old LRP6 KO mice had a significant reduction in bone mass in the femora secondary spongiosa relative to their wild type littermates, whereas marginal changes were seen in femoral tissue of 1 month-old LRP6 KO mice. The remodeling area of the 3 month-old LRP6 KO mice showed a decreased bone formation rate as detected by Goldner's Trichrome staining and calcein double labeling. Bone histomorphometric and immumohistochemical analysis revealed a reduction in osteoblasts but little change in the numbers of osteoclasts and osteoprogenitors/osteoblast precursors in LRP6 KO mice compared to wild type littermates. In addition, the percentage of the apoptotic osteoblasts on the bone surface was higher in LRP6 KO mice compared to wild type littermates. Intermittent injection of PTH had no effect on bone mass nor osteoblastic bone formation in either trabecular and cortical bone in LRP6 KO mice, whereas all were enhanced in wild type littermates. Additionally, the anti-apoptotic effect of PTH on osteoblasts in LRP6 KO mice was less significant compared to wild type mice. Therefore, our findings demonstrate that LRP6 in osteoblasts is essential for osteoblastic differentiation during bone remodeling and the anabolic effects of PTH.

Keywords

LRP6; PTH; bone remodeling; osteoblast differentiation; osteoblast apoptosis

Introduction

The regulation of bone mass, or bone remodeling in adults, is a dynamic process orchestrated by bone-forming osteoblasts and bone-resorbing osteoclasts. Growth factors

*Corresponding author: Mei Wan, Ross Building, Room 229, 720 Rutland, Avenue, Baltimore, MD 21205, Telephone: (410) 502-6598, Fax: (410) 502-6239, mwan4@jhmi.edu.

Disclosure

All authors state that they have no conflicts of interest.

Authors' roles: MW designed the experiments. CL, QX, BY, HX, WW, and CS carried out the experiments and analyzed the data. MW wrote the paper. XC and JC edited the manuscript.

such as active TGFβ and IGF-1 are released during osteoclastic bone resorption to recruit mesenchymal stem cells (MSCs) and promote their differentiation to osteoblasts to couple new bone formation to bone resorption (1–3). An imbalance of osteoblastic bone formation and osteoclastic bone resorption leads to bone disorders such as osteoporosis. Parathyroid hormone (PTH) stimulates bone remodeling and is the only FDA-approved anabolic therapy for osteoporosis as intermittent administration of PTH selectively stimulates bone formation (4–6). The bone anabolic effect of PTH also has been demonstrated extensively in mice and rats (7). Histologic studies have shown that the increase in bone formation is largely due to an increase in the number of matrix-synthesizing osteoblasts (7;8). However, the signaling mechanisms responsible for PTH-mediated effects on bone are still incompletely understood as the traditional signaling pathway of cyclic AMP (cAMP) production and protein kinase A (PKA) activation does not provide a satisfactory explanation for all the anabolic effects of PTH.

Low-density lipoprotein receptor-related protein 5 and 6 (LRP5 and 6) are primarily known for their key role in mediating the transduction of signals from secreted Wnt proteins to β-catenin (9–13). Although they have similar structures, several lines of evidence suggest that LRP5 and LRP6 may have unique roles regarding skeletal growth and bone remodeling. Mutations in *LRP5* or *LRP6* are associated with distinct phenotypes of skeletal diseases. Inactivation of *LRP5* was identified as the causative genetic alteration underlying Osteoporosis-Pseudoglioma Syndrome (OPPG) (14), a rare syndrome associated with premature, generalized osteoporosis leading to bone fracturing and progressive blindness. A gain-of-function mutation in LRP5 (G171V) has been identified in individuals displaying high-bone-mass (15–17). Individuals with a *LRP6* mutation show early coronary disease and severe osteoporosis (18). A common protein variant of LRP6 (Ile1062Val) is associated with fracture risk in elderly men (19;20). Mouse genetic studies also reveal distinct roles LRP5 and LRP6 in bone. *Lrp5* knockout mice are viable but suffer from osteoporosis in adulthood (21). In contrast, *Lrp6* knockout mice are perinatal lethal due to developmental abnormalities like truncations of the axial skeleton, limb defects, and loss of the paraxial mesoderm (10;22). The analysis of the phenotypes of mice carrying heterozygous mutations of *Lrp6* and either heterozygous or homozygous mutations of *Lrp5* show that Lrp6 participates in the control of bone mass accrual in a manner that suggests more than a simple redundancy with *Lrp5* (23). These studies suggest that LRP6 is involved in both bone development and bone remodeling in adults.

We have previously found that PTH orchestrates the signaling pathways of different growth factors, such as Wnts, TGFβ and BMPs, that directly regulate osteoblast differentiation and function (24–26). Particularly, PTH stabilizes β-catenin through LRP6 (24). LRP6 is also required for PTH-mediated cAMP production (27). PTH promotes the interaction of the cytoplasmic domain of LRP6, but not LRP5, with $G\alpha_s\beta\gamma$ to set up a functional PTH1R-$G\alpha_s$-adenylate cyclase complex for the rapid production of cAMP and subsequent PKA activation. Furthermore, we recently found that LRP6 in MSCs acts as a negative regulator for BMP-induced MSC commitment to the osteoblastic lineage. PTH disrupts the LRP6-organized extracellular antagonist network by inducing endocytosis of a PTH1R-LRP6-antagonist complex, resulting in increased commitment and differentiation of MSCs to osteoblasts (26). Notably, PTH-stimulated bone formation can still occur in LRP5-deficient mice (28;29), indicating that LRP5 is not required for PTH anabolic actions in bone. Collectively, these findings suggest that LRP6 specifically is a key element in PTH-mediated signaling pathways enhancing osteoblastic numbers and function.

It is known that PTH enhances the number and the activation of osteoblasts through increasing osteoblast proliferation and differentiation, and decreasing osteoblast apoptosis (7;8;30;31). As LRP6 is a key element in PTH-elicited cAMP/PKA and β-catenin signaling,

it may mediate the effects of PTH on osteoblasts and its positive effect on bone formation. Here we systemically analyzed the function of LRP6 in bone remodeling in osteoblast-specific LRP6-deficient mice. We found that LRP6 in osteoblasts is required for osteoblast differentiation and survival during bone remodeling in adult mice. Importantly, PTH anabolic effects were blunted in the LRP6 KO mice.

Materials and Methods

Antibodies and reagents

Primary antibodies including goat anti-LRP6 (Abcam), rabbit anti-osterix (Abcam), rabbit anti-osteocalcin (Takara), mouse anti β-catenin (BD Biosciences), and rat anti-BrdU (Abcam) were used for immunohistochemical analysis. Secondary antibodies for immunohistochemistry were from Jackson ImmunoResearch. Human PTH(1–34) was purchased from Bachem Bioscience Inc. Adenovirus-GFP (Ad-GFP) and Adenovirus-Cre (Ad-Cre) recombinant adenovirus were purchased from Vector Laboratories.

LRP6 conditional null mice and PTH treatment

Lrp6$^{f/f}$ mice were obtained from Van Andel Research Institute (32;33). Transgenic mice expressing the Cre recombinase under the control of a 3.9-kb fragment of the human osteocalcin promoter (*Oc-Cre*), created in a Friend leukemia virus strain B genetic background, were obtained from T. Clemens (Baltimore, MD) (34). LRP6$^{f/f}$ mice were crossed with *Oc-Cre* mice to generate *Oc-Cre*; *Lrp6*$^{f/f}$ progeny, which were used in subsequent mating. The animals that had a genotype of *Cre*$^{-/-}$;*LRP6*$^{f/f}$ were considered control (WT), and *Cre*$^{+/-}$;*LRP6*$^{f/f}$ were considered LRP6 deletion (KO). All animals were maintained in the Animal Facility of the Johns Hopkins University School of Medicine. The experimental protocol was reviewed and approved by the Institutional Animal Care and Use Committee of the Johns Hopkins University, Baltimore, MD, USA. Genomic DNA was extracted from tail snips with phenol/chloroform. Genotyping of the animals was achieved by PCR for Cre recombinase (5'-CAAATAGCCCTGGCAGAT-3' and 5'-TGATACAAGGGACATCTTCC-3') and the loxP sites (5´-GGGGTTCTACTTTTGTGTGTGG −3´ and 5´- CCGTCTGTTTGCATAAAGCAACA −3´). For PTH treatment, two month-old male Cre$^{-/-}$;LRP6$^{f/f}$ (WT) and Cre$^{+/-}$;LRP6$^{f/f}$ (KO) mice were randomized into four groups: WT-Vehicle, WT-PTH, KO-vehicle, and KO-PTH. Ten mice of each treatment group were used. Mice were treated daily, five days per week, with either vehicle (1mM acetic acid in PBS) or human PTH1-34 at a dose of 80 μg/kg with subcutaneous injection for 4 weeks.

Analysis of skeletal phenotypes

Mice were anesthetized by inhalation of 2.5% isoflurane (Abbott Laboratories, Abbott Park, IL, USA) mixed with O_2 (1.5 liters/minute). For μCT analysis, femora obtained from mice were dissected free of soft tissue, fixed overnight in 70% ethanol and analyzed by a high resolution μCT (SkyScan1076 in-vivo CT, SKYSCAN company). Image Reconstruction software (NRecon v1.6), data analysis software (CTAn v1.9), and three-dimensional model visualization software (CTVol v2.0) were used to analyze parameters of the trabecular bone in the metaphysis and mid-diaphyseal cortical bone. The scanner was set at a voltage of 50 kVp, a current of 201 μA and a resolution of 12.63679 μm per pixel. Cross-sectional images of the distal femur were used to perform three-dimensional histomorphometric analysis of trabecular bone. For 1 month-old mice, the sample area selected for scanning was a 2.0-mm length of the metaphyseal trabecular bone immediately subjacent to the growth plate. For 3 month-old mice, the sample area selected for scanning was a 2.0-mm length of the metaphyseal secondary spongiosa, originating 1.0 mm below the lowest point of growth plate (illustrated in Fig. 1E). Cortical morphometry was analyzed within a 600 μm long

section at mid-diaphysis of the femur and included measurements of average thickness and cross-sectional area.

For histochemistry, immunohistochemistry, and histomorphometric analysis, the femora were resected and fixed in phosphate-buffered saline (pH 7.4) containing 4% paraformaldehyde for 48 hours, decalcified in 10% ethylenediamine tetraacetic acid (EDTA) (pH 7.0) for 14 days and embedded in paraffin. Four-μm-thick longitudinally oriented sections of bone including the metaphysis and diaphysis were processed for hematoxylin-eosin and immunohistochemical staining. For static histomorphometry, measurements of two-dimensional parameters of the trabecular bone were performed with OsteoMeasureXP Software (OsteoMetrics, Inc.). For 1 month-old mice, the sample area selected for calculation was a 1 mm^2 area within the metaphyseal trabecular bone. For 3 month-old mice, the sample area selected for scanning was a 1 mm^2 area within the metaphyseal secondary spongiosa. All sections were observed on Olympus BX51 microscope. For dynamic histomorphometry, two sequential doses of calcein (8 mg/10 ml sterile saline) were injected intraperitoneally at 3 and 10 days prior to sacrifice. Bone histomorphometry analysis in undecalcified femoral sections was performed by OsteoMeasure system (OsteoMetrics, Inc.).

Immunohistochemistry analysis was performed using standard protocol as the manufacturer recommended (EnVision™ System, Dako, USA). Briefly, the bone sections were processed for antigen retrieval by digestion in 0.05% trypsin (pH 7.8) for 15 minutes at 37°C, and then incubated with antibodies against LRP6 (diluted 1:50), osteocalcin (Ser463/465) (diluted 1:100), osterix (diluted 1:400), BrdU (diluted 1:100), and β-catenin (diluted 1:100) overnight at 4 °C. An HRP-streptavidin detection system (Dako) was subsequently used to detect the immunoactivity followed by counterstaining with hematoxylin (Sigma). Sections incubated with 1% nonimmune serum PBS solution served as negative controls.

TUNEL assays were performed using parafin-embedded bone sections. Apoptotic cells were detected using DeadEnd™ Colorimetric Apoptosis Detection System (Promega, Madison, WI) according to manufacturer instructions.

Measurements of serum osteocalcin and cross-linked C terminal telopeptide of type 1 collagen (CTX-I)

Serum bone formation marker osteocalcin and bone resorption marker CTX-I, were measured using commercial kits: Mouse Osteocalcin EIA Kit (Biomedical technologies, Inc. Stoughton, MA) and Mouse CTX-I ELISA Kit (MyBioSource, Inc., San Diego, CA) according to the manufacturer's instructions.

Primary osteoblast culture and adenovirus infection

Calvaria (frontal and parietal bones) was removed from newborn (5~6 day-old) *LRP6*$^{f/f}$ mice aseptically. After removal of sutures, the calvariae were subjected to serial digestions in 1.0 mg/ml of collagenase type IV (Sigma). Briefly, calvaria were digested in 10 ml of digestion solution for 15 minutes at 37°C under constant agitation. The digestion solution was then collected, and the digestion was repeated an additional 4 times. Digestion solutions 3–5, which contained the osteoblasts, were pooled together. After centrifugation at 600g for 10 min, the fractions were resuspended in α-Minimum Essential Medium (α-MEM) containing 10% Fetal Calf Serum (FCS), and filtered through a 70-mm cell strainer. Osteoblasts were obtained and cultured in α-MEM containing 10% FCS and 1% penicillin/streptomycin at 37°C in a humidified incubator supplied with 5% CO_2. To eliminate LRP6 from the cells, monolayer osteoblasts were infected with control adenovirus (Ad-GFP) or

Cre recombinase virus M1 (Ad-CreM1) (Vector Laboratories) at a multiplicity of infection (MOI) of 100 for most experiments.

Quantitative Real-Time PCR (qRT-PCR)

Total RNA for qRT-PCR was extracted from bone tissue and cultured cells using Trizol reagent (Invitrogen) according to the manufacturer's protocol. For qRT-PCR, cDNA was prepared with random primers using the SuperScript First-Strand Synthesis System (Invitrogen) and analyzed with SYBR GreenMaster Mix (QIAGEN) in the thermal cycler with two sets of primers specific for each targeted gene. Relative expression was calculated for each gene by 2-CT method with GAPDH for normalization. Primers used for qRT-PCR were: Col1A (5'-GCGAAGGCAACAGTCGCT-3') and (5'-CTTGGTGGTTTTGTATTCGATGAC-3'); Osteocalcin (5'-CTGACCTCACAGATCCCAAGC-3') and (5'-TGGTCTGATAGCTCGTCACAAG-3') ; bone sialoprotein (BSP) (5'-TACCGGCCACGCTACTTTCTTTAT-3') and (5'-GACCGCCAGCTCGTTTTCATCC-3') ; dentin matrx protein-1 (DMP1) (5'-GGCTGTCCTGTGCTCTCCCAG-3') and (5'-GGTCACTATTTGCCTGTGCCTC-3'); Axin2 (5'-ATGAGTAGCGCCGTGTTAGTG-3') and (5'-GGGCATAGGTTTGGTGGACT-3'); Naked2 (5'-GGGACGACAAGGGTTCCCTA-3') and (5'-AGTGCGTCAATGTTCAAGTGC-3'); bone morphogenetic protein-4 (BMP4) (5'-TTGATACCTGAGACCGGGAAG-3') and (5'-ACATCTGTAGAAGTGTCGCCTC-3'); osteoprotegrin (OPG) (5'-GTGAAGCAGGAGTGCAAC-3') and (5'-GCAAACTGTGTTTCGCTC-3'); receptor activator of nuclear factor kappa-B ligand (RANKL) (5'-TGTACTTTCGAGCGCAGATG-3') and (5'-ACATCCAACCATGAGCCTTC-3'); matrix metalloprotein 13 (MMP13) (5'-GGTCCCAAACGAACTTAACTTAC-3') and (5'-CCTTGAACGTCATCATCAGGAAG-3'); c-JUN (5'-GCCAACATGCTCAGGGAACAGGT-3') and (5'-GCCCCTCAGCCCTGACAGTCTG-3'), c-fos (5'-AATGGTGAAGACCGTGTCAGGA-3') and (5'-CCCTTCGGATTCTCCGTT TCT-3'); and GAPDH (5'-AGGTCGGTGTGAACGGATTTG-3') and (5'-GGGGTCGTTGATGGCAACA-3').

Statistical analysis

All data were presented as mean ± SEM. For comparison of histomorphometric parameters in WT and KO mice, Student's *t*-test was used. For quantitative analysis of immunostaining data, Student's *t*-test was performed followed by Chi-square Test. Significant level was defined as $P < 0.05$.

Results

Bone mass is decreased in adult mice with Oc-Cre-mediated conditional LRP6 deletion

To determine the role of LRP6 in osteoblastic bone formation, we generated mice lacking *Lrp6* specifically in mature osteoblasts (Oc-Cre; $Lrp6^{f/f}$, named "KO" hereafter) using *Cre*-mediated recombination. Transgenic mice expressing the *Cre* recombinase driven by the human osteocalcin promoter were crossed with homozygous mice that expressed *loxP*-flanked *Lrp6* ($Lrp6^{f/f}$). To confirm that LRP6 deletion in KO mice was specific to osteoblasts, we performed PCR analysis using a combination of primers that specifically detected floxed *Lrp6* alleles ($Lrp6^{f}$) and null alleles ($Lrp6^{\Delta}$). Genomic DNA was extracted from skeletal tissues including calvariae, femur, and spine as well as several non-skeletal tissues such as brain, kidney, lung, liver, heart, and muscle from the KO mice. *Cre*-mediated recombination occurred exclusively in tissues that contained osteoblastic cells, whereas non-skeletal tissues retained the intact *Lrp6*-floxed alleles ($Lrp6^{f}$) (Fig. 1A). LRP6-positive

osteoblasts in femur tissue were also detected by immunohistochemical analysis of tissue sections using an antibody against LRP6. While 58.6% of the bone surface osteoblasts expressed LRP6 in LRP6$^{f/f}$ mice (named "WT" hereafter), almost none of the osteoblasts expressed LRP6 in KO mice (Fig. 1B and Supplemental Fig. S1). No significant reduction of LRP6-positive cell numbers in bone marrow was observed in KO mice compared to WT mice (Fig. 1C and Supplemental Fig. S1). Thus, LRP6 deficiency was limited to mature osteoblasts on the bone surface. KO mice were born at the expected Mendelian frequency, and all exhibited survival indistinguishable from that of WT mice. Mice expressing cre only did not exhibit any skeletal abnormality relative to wild type mice in deferent studies (34;35) and no abnormal phenotype was observed in our analysis (data not shown). The body weight and femoral length were not decreased in either male or female KO mice compared with WT controls at 1 and 3 months of age (Table 1).

To dissect the role of LRP6 in osteoblast differentiation in bone growth and remodeling, we analyzed the femora bone phenotypes of young (1 month-old) and adult (3 month-old) mice. One month-old KO mice did not exhibit significant differences in trabecular bone volume, number, thickness or separation relative to their WT littermates as measured by μCT (Fig. 1D–1H). However, 3 month-old KO mice showed reduced trabecular bone volume and number, and greater trabecular bone separation in the secondary spongiosa area compard to WT littermates (Fig. 1D–1H). No significant differences were observed for the cortical bone parameters including bone area, bone area/total area, and cortical bone thickness in both 1 and 3 month-old KO mice as compared to their WT littermates (Fig. 1I–1M). The results suggest that LRP6 deficiency in mature osteoblasts primarily affected trabecular bone remodeling in adults.

Bone formation, but not bone resportion, is impaired in mice with Oc-Cre-mediated conditional LRP6 deletion

Bone histomorphometric analyses of femora revealed no changes in the number of osteoblasts and osteoclasts in 1 month-old KO mice (Fig. 2A–2D). A reduced number of osteoblasts but no change in the numbers of osteoclasts was observed in 3 month-old KO mice as compared to their WT littermates (Fig. 2E–2H). Reduced bone formation in 3 month-old KO mice was also confirmed by Goldner's Trichrome staining and double calcein labeling analysis (Fig. 2I-K). Distal femur showed a decrease in bone volume (*green*/*blue*) and newly formed bone (*red*) (Fig. 2I). We analyzed dynamic changes in bone remodeling by injecting calcein twice at 7-day intervals before euthanizing the animals. The distance between two consecutive labels in the trabecular bone of the femur was less in KO mice than in the WT controls (Fig. 2J). Quantification of these parameters demonstrated that KO mice had reduced BRF/BS when compared to WT littermates (Fig. 2K). To investigate if osteoclast bone resorption activities were affected, we performed TRAP staining in the femoral sections of 3 month-old mice. The number of TRAP-positive osteoclasts on the trabecular bone surface of KO mice was unchanged compared to WT mice (Fig. 2L and 2M). We then examined whether β-catenin signaling was affected by LRP6 deficiency in osteoblasts. We analyzed β-catenin target gene expression in femora bone tissue. Axin2 (36–38), Naked2 (39;40), BMP4 (41) and OPG (42;43) were significantly down-regulated by 30–40% in KO mice relative to WT mice (Fig. 2N–2Q). Of note, RANKL expression was also decreased in KO mice (Fig. 2R). Overall, the ratio of OPG/RANKL was maintained (Fig. 2S) in KO mice compared to WT littermates, which may be the main reason why osteoclastic bone resorption was not affected. Taken together, these results demonstrate that deletion of LRP6 in osteoblasts impaired bone formation without affecting osteoclastic bone resorption during bone remodeling in adult mice.

Oc-Cre-mediated conditional LRP6 deletion leads to decreased expression of osteoblast differentiation genes and accelerated osteoblast apoptosis during bone remodeling

To explore the cellular mechanism underlying the reduced osteoblastic bone formation observed in the KO mice, we examined osteogenic gene expression in the femoral trabecular bone tissue of 3 month-old LRP6 KO mice. Bone surface osteocalcin^{+}- and osterix^{+} -osteoblast numbers in the second spongiosa of KO mice were significantly reduced relative to WT mice (Fig. 3A, 3B, Supplemental Fig. S2A, and S2B). Consistently, the number of osteocytes, representing terminal differentiation of the osteoblast lineage, was also significantly reduced in the trabecular bone matrix of KO mice relative to their WT littermates (Fig. 3C and Supplemental Fig. S2C). The mRNA expression levels as assessed by qRT-PCR of bone matrix proteins produced by mature osteoblasts (Col1A, osteocalcin, and BSP) and osteocytes (DMP1) were also decreased in bone tissue from 3 month-old KO mice (Fig. 3E). The expression levels of these genes were not changed in 1 month-old mice compared to their age-matched WT controls (Fig. 3D). We next sought to determine whether deletion of LRP6 in osteoblasts affected proliferation and/or apoptosis of osteoblasts in the secondary spongiosa area during bone remodeling. Analysis of BrdU labeling revealed that the proliferation of bone surface osteoblasts and bone matrix osteocytes in the second spongiosa of KO mice was not different from that of WT mice (Fig. 3F and Supplemental Fig. S2D). However, the percentage of apoptotic osteoblasts on the bone surface was greater in LRP6 KO mice relative to their WT littermates as detected by TUNEL assay (Fig. 3G and Supplemental Fig. S2E). In the bone marrow of the secondary spongiosa, TUNEL^{+} cells (Fig. 3H and Supplemental Fig. S2E) and Osterix^{+} osteoprogenitors (Fig. 3I and Supplemental Fig. S2B) were not changed in KO mice relative to their WT littermates. These results indicate that LRP6 deficiency in osteoblasts resulted from increased apoptosis, decreasing the number of bone surface osteoblasts, but did not affect the pool of osteoblasts-deriving osteoprogenitors during bone remodeling.

Oc-Cre-mediated LRP6 deficient mice exhibit a blunted response in bone formation to PTH treatment

To determine whether LRP6 in osteoblasts is required for PTH anabolic effects on bone, 2 month-old male KO mice and littermate WT controls were treated with PTH1–34 for 4 weeks. Femora trabecular and cortical bone was analyzed by μCT and histomorphometry. In WT mice, PTH increased bone mass in trabecular and cortical bone (Fig. 4A and Supplemental Fig. S3). Particularly, PTH1–34 increased BV/TV (Fig. 4B), BMD (Fig. 4C), Tb.N (Fig. 4D), Tb.Th (Fig. 4F), and decreased Tb.Sp (Fig. 4E) in WT mice compared to the vehicle-treated WT mice. However, these PTH-induced changes were not seen in KO mice and actually resulted in a decreased BMD compared to the vehicle-treated KO mice. Goldner's Trichrome staining revealed increased newly formed bone (red) with PTH1–34 treatment only in WT mice, not in KO mice compared to their respective vehicle-treated controls (Fig. 4G). The capacity of PTH1–34 treatment to increase the amount of bone deposited between two timed administrations of calcein labeling, an indicator of bone mineralization in WT mice, was diminished in KO mice (Fig. 4H and 4I). Quantification of these calcein intervals revealed that the in absence of LRP6, PTH1–34 treatment did not change the mineral apposition rate (MAR) in KO mice, whereas the MAR was increased in the PTH1–34-treated WT mice compared to their respective vehicle-treated controls (Fig. 4J), suggesting decreased activity of individual osteoblasts. Analyses of dynamic parameters of bone formation further indicated that PTH1–34 increased the bone formation rate over the bone surface (BFR/BS), which reflects the quantity of osteoblasts forming the bone matrix, in WT mice but not in KO mice (Fig. 4K). Thus, the PTH anabolic effects were abrogated by LRP6 deletion in osteoblasts.

Oc-Cre-mediated LRP6 deficient mice exhibit blunted osteoblast differentiation and anti-apoptotic responses to PTH

Given that the anabolic effect of PTH results from a tight balance between osteoblastic bone formation and osteoclastic bone resorption (7;44), we then investigated whether LRP6 deficiency impairs PTH-stimulated bone formation only or both osteoblastic bone formation and osteoclastic bone resorption. Analysis of the secondary spongiosa by bone histomorphometry revealed that the two static indices of bone formation stimulated by PTH, the number of osteoblasts per bone surface (N.Ob/B.Pm) (Fig. 5A) and the percentage of surfaces covered by osteoblasts (Ob.S/BS) (Fig. 5B), were only observed in WT mice but not in KO mice. On the contrary, the two indices of trabecular bone resportion, the number of osteoclasts per bone surface (N. Oc/B. Pm) (Fig. 5C) and the percentage of surfaces covered by osteoclasts (Oc.S/BS) (Fig. 5D), increased by a similar extent in WT and KO mice in response to PTH1–34 treatment compared to their respective vehicle-treated controls. Consistently, Oc-Cre-mediated LRP6 deficiency blunted the increase in number of osteocalcin$^+$ osteoblasts on the bone surface (Fig. 5E and 5F) but did not change the effect of increased number of TRAP$^+$ osteoclasts stimulated by PTH1–34 in KO mice (Fig. 5G and Fig. 5H). We also measured serum concentrations of osteocalcin and CTX-I in response to PTH1–34 treatment. The levels of both serum osteocalcin and CTX-I in WT and KO mice increased significantly in the PTH-treated groups compared to the vehicle-treated groups. However, the serum osteocalcin concentration was not stimulated in PTH-treated KO mice as significantly as in PTH-treated WT mice, whereas the PTH-stimulated increase in serum CTX-I concentration was similar in the KO and WT mice (Fig. 5I and 5J). Thus, LRP6-mediated signaling in mature osteoblasts is important for osteoblast differentiation during bone remodeling and PTH-stimulated bone formation.

We next examined whether LRP6 deletion in osteoblasts affects the number of osterix-positive cells, which are osteoblast-deriving osteoprogenitors, by immunohistochemical analysis. In WT mice, PTH significantly increased osterix$^+$ osteoprogenitors in both bone marrow and on the bone surface (Fig. 6A–6C). On the contrary, in KO mice, although PTH was able to increase the number of osterix$^+$ osteoprogenitors in the bone marrow, PTH failed to increase the number of bone surface osterix$^+$ cells compared to vehicle treatment (Fig. 6A–6C), indicating that deletion of LRP6 in osteoblasts does not affect the pool of osteoblast-deriving bone marrow osteoprogenitors but likely impairs the recruitment, terminal differentiation and/or survival. As an increased number of apoptotic osteoblasts on the bone surface was observed in KO mice (Fig. 3G and Supplemental Fig. S2E) and PTH has previously been shown to have anti-apoptotic effects, we examined whether LRP6 deletion in osteoblasts affects PTH-inhibition of osteoblast apoptosis. The percentage of apoptotic osteoblasts on bone surface was reduced by PTH treatment in WT mice, consistent with previous reports (7;45;46). However, the anti-apoptotic effect of PTH was abrogated by LRP6 deletion (Fig. 6D and 6E). These results suggest that LRP6 is required for osteoblast survival in PTH-stimulated bone remodeling.

PTH failed to stimulate β-catenin and $G\alpha_s$-PKA signaling in LRP6-deficient osteoblasts

Finally, we sought to determine whether PTH-activated signaling pathways are affected by the deletion of LRP6 in osteoblasts. We previously found that LRP6 is essential for PTH stimulated β-catenin signaling, a positive regulator in bone formation, in osteoblasts (24). We tested whether LRP6 deficiency would affect β-catenin signaling activation induced by PTH in osteoblasts. Consistent with our previous report (24), PTH1–34 significantly increased β-catenin$^+$ osteoblasts on bone surface in secondary spongiosa of WT mice (Fig. 7A and 7B). β-catenin$^+$ osteoblasts on bone surface in the same area in KO mice did not increase in response to PTH1–34 treatment compared to vehicle-treated controls (Fig. 7A and 7B). In addition, the PTH-stimulated increased expression of β-catenin target genes

Naked2 and Axin1 was reduced in LRP6-deficient PTH-treated calvarial osteoblasts compared with those in WT calvarial osteoblasts (Fig. 7C). We previously also demonstrated that LRP6 mediates PTH-activated $G\alpha_s$-PKA signaling activation in osteoblasts (27). We detected the mRNA expression of c-JUN, c-fos (47–49), and MMP13 (50;51), genes stimulated by PTH through $G\alpha_s$-PKA-dependent pathway. LRP6-deficiency in osteoblasts reduced the relative abundance of PTH-stimulated c-fos, RANKL, and MMP13 gene expression in isolated cavarial preosteoblasts compared to PTH-treated WT osteoblasts (Fig. 7C). The results suggest that Oc-Cre mediated conditional LRP6 deletion alleviated both β-catenin signaling and $G\alpha_s$-PKA signaling activation stimulated by PTH in osteoblasts.

Discussion

Mutations in both LRP5 and LRP6 have been linked to changes in bone mass in humans and mice, but the role of LRP6 in bone metabolism has not been studied as extensively relative to that of LRP5. In addition to its role in wnt-canonical pathway signaling, LRP6 is also required for PTH-stimulated signaling pathways in osteoblasts (24;27). Whether or not LRP6 mediates PTH anabolic bone effects *in vivo* has not been investigated. Here we demonstrate that LRP6 deficiency in mature osteoblasts decreased bone formation in the secondary spongiosa area in 3 month-old adult mice that have active bone remodeling, but had marginal effects on bone acquisition in young mice. Further, the body weight and femur length in 1 month-old LRP6-deficient mice of both sexes were not reduced in comparison with those of wild type littermates. Thus, osteoblast-specific LRP6 is required for bone formation specifically during bone remodeling, and is most likely not critical in bone development and postnatal growth. In addition, the anabolic effect of intermittent PTH administration during bone remodeling was abolished in osteoblast-specific LRP6-deficient mice. These *in vivo* evidence and the previous finding that intermittent PTH treatment was fully anabolic in LRP5-deficient mice (13;14) consistently support the concept that LRP6, but not LRP5, is an essential mediator for PTH-elicited bone anabolic effect during bone remodeling.

Bone remodeling is mediated by tight coupling of osteoclastic bone resorption on the bone surface and osteoblastic new bone formation at the same sites. In the coupling process, local factors released and activated during osteoclastic bone resorption induce the migration of MSCs/osteoprogenitors to the remodeling bone surface where they differentiate into mature osteoblasts to form new bone (1–3). Our results show that LRP6 is required for osteoblast differentiation and survival during the recruitment of osteoblasts in the remodeling process. Indeed, mRNA levels of the osteoblast differentation markers were reduced in bone tissue of 3 month-old LRP6-deficient mice, whereas the levels of these genes were maintained in 1 month-old LRP6-deficient mice. Further analysis of the cellular changes in the secondary spongiosa of the femur of LRP6 KO mice revealed a dramatically reduced number of osteoblasts and increased number of apoptotic osteoblasts on the bone surface, indicating that LRP6 is necessary for the survival of osteoblastic cells during bone remodeling. PTH produces osteoanabolic activity via anti-apoptotic mechanisms in osteoblasts, and increased cell survival is one of the major contributors to the increased number of osteoblasts caused by PTH (7). Our demonstration that deletion of LRP6 abolished the anti-apoptotic effect of PTH on osteoblasts suggests that LRP6 is involved in PTH anti-apoptotic effect in osteoblasts. While the molecular mechanisms by which LRP6 regulates osteoblast apoptosis remain to be determined, it has been reported that the attenuation of osteoblast apoptosis by PTH requires PKA-mediated phosphorylation (7;45;46). Our results showed that the expression of PKA downstream target genes stimulated by PTH such as c-fos, RANKL, and MMP13 were abolished in LRP6-deficient osteoblasts, indicating that LRP6-deficiency may promote osteoblast apoptosis through disruption of PTH-stimulated PKA signaling.

Interestingly, LRP6 deletion did not affect osteoblast differentiation and bone formation during bone development and growth. LRP6, containing a large extracellular domain, has been proposed to act as a central organizer for the extracellular antagonist network for the regulation of signaling pathways of different local growth factors (26). Different types and levels of extracellular factors produced may differentially influence the effect of LRP6 in osteoblasts. The extracellular bone marrow microenvironment in bone growth is different from that of bone remodeling, which involves osteoclast bone resorption and release of matrix factors. Mice with LRP6 deletion in early mesenchyme exhibited relatively normal skeleton (33), providing additional evidence for the dispensable role of LRP6 in bone formation during development.

LRP6 deletion in osteoblasts did not affect osteoclastogenesis as indicated by normal osteoclast numbers, normal $TRAP^+$ cell numbers on bone surface, and normal serum CTX-I concentrations relative to wild type mice. On the other hand, our results from the current study strongly support our previous finding that LRP6 is a key mediator for PTH activated-β-catenin signaling in osteoblasts (24) as deletion of LRP6 resulted in reduced expression of downstream target genes of β-catenin signaling in bone tissue. It is known that deletion of β-catenin within mature osteoblasts causes a decrease in OPG production and an increase in osteoclast activity (42;43;52). Consistently, we found LRP6 KO mice to have decreased expression of OPG. It is also known that RANKL is a direct target gene of PKA signaling in osteoblasts (53–55). We found that PTH lost its ability to stimulate PKA signaling in osteoblasts in LRP6 KO mice, which may be a major contributor to our observation of reduced RANKL production in osteoblasts. Thus, downregulation of OPG and RANKL separately caused by suppressed β-catenin and PKA signaling, may reach a balance to maintain the osteoclast activity in LRP6 KO mice and explain the normal ratio we observed of RANKL/OPG compared to WT controls. This finding provides one possible explanation for the different bone phenotypes derived from the β-catenin-deficiency (42;43;52) and our findings with LRP6-deficiency. Our results also suggest that LRP6 is required for both PTH-stimulated β-catenin and PKA signaling, which most likely play different roles in regulating osteoblast and osteoclast activities. PTH directly stimulates PKA signaling activation, which subsequently phosphorylates transcription factors, such as Cbfa1 and cAMP-response element-binding protein (CREB), regulating the transcription of many genes and multiple cellular activities including osteoblast differentiation, survival/apoptosis, cell cycle, proliferation, and osteoclast activity (7;56;57). PTH can also activate β-catenin signaling in osteoblasts and thereby regulate the activity of osteoclasts. Additionally, PTH stimulates many other signaling pathways such as PKC, MAPK, etc. It remains to be determined whether LRP6 is involved in the activation of these signaling pathways in osteoblasts. In addition to PTH signaling, LRP6 may also be involved in other growth factor/cytokine-stimulated RANKL production in osteoblasts, which is another interesting topic for future study. Nevertheless, we have found that LRP6 in osteoblasts is not only a mediator for β-catenin signaling activation, but regulates the functions of osteoblasts and osteoclasts through distinct PTH-signaling mechanisms.

One of the functions of PTH is to promote the commitment and differentiation of MSCs or osteoprogenitors into mature osteoblasts (7;58;59). BMP-induced MSC commitment to osteoblastic lineage was suppressed by LRP6 via extracellular antagonist network, which can be disrupted by PTH-induced endocytosis of the PTH1R-LRP6 complex, resulting in increased commitment of MSCs to the osteoblastic lineage (26). Further characterization of the role of MSC- or osteoprogenitor-specific LRP6 mediated signaling in bone remodeling using nestin-Cre or osterix-Cre mouse models are needed. Whether PTH still stimulates bone formation in these mouse models is also worth testing. MSCs are one of the major constituents of the bone marrow microenvironment that supports hematopoietic stem cells (58–60). It is known that intermittent PTH treatment expands hematopoietic stem and

progenitor cells (61;62). MSCs have been shown to express PTH receptors and to increase in number and undergo redistribution in bone marrow upon PTH treatment. Therefore, examining whether LRP6 plays a role in PTH-regulated stem cell behavior in bone marrow is another interesting topic for future study.

In conclusion, our studies demonstrate that LRP6 in osteoblasts is a positive regulator for osteoblastic bone formation during bone remodeling and plays a critical role in the osteoanabolic action of PTH.

Supplementary Material

Refer to Web version on PubMed Central for supplementary material.

Acknowledgments

This work was supported by National Institutes of Health Grant DK083350 to M. W. We thank Bart O. Williams (Van Andel Research Institute) for providing the $LRP6^{f/f}$ mice. We thank Ryan Riddle (Johns Hopkins University School of Medicine) for providing the primers for qRT-PCR analysis of OPG and RANKL.

References

1. Tang Y, Wu X, Lei W, Pang L, Wan C, Shi Z, Zhao L, Nagy TR, Peng X, Hu J, Feng X, Van HW, Wan M, Cao X. TGF-beta1-induced migration of bone mesenchymal stem cells couples bone resorption with formation. Nat Med. Jul.2009 15:757–765. [PubMed: 19584867]
2. Wu X, Pang L, Lei W, Lu W, Li J, Li Z, Frassica FJ, Chen X, Wan M, Cao X. Inhibition of Sca-1-positive skeletal stem cell recruitment by alendronate blunts the anabolic effects of parathyroid hormone on bone remodeling. Cell Stem Cell. Nov 5.2010 7:571–580. [PubMed: 21040899]
3. Xian L, Wu X, Pang L, Lou M, Rosen CJ, Qiu T, Crane J, Frassica F, Zhang L, Rodriguez JP, Xiaofeng J, Shoshana Y, Shouhong X, Argiris E, Mei W, Xu C. Matrix IGF-1 maintains bone mass by activation of mTOR in mesenchymal stem cells. Nat Med. Jul.2012 18:1095–1101. [PubMed: 22729283]
4. Murray TM, Rao LG, Divieti P, Bringhurst FR. Parathyroid hormone secretion and action: evidence for discrete receptors for the carboxyl-terminal region and related biological actions of carboxyl-terminal ligands. Endocr Rev. Feb.2005 26:78–113. [PubMed: 15689574]
5. Hodsman AB, Bauer DC, Dempster DW, Dian L, Hanley DA, Harris ST, Kendler DL, McClung MR, Miller PD, Olszynski WP, Orwoll E, Yuen CK. Parathyroid hormone and teriparatide for the treatment of osteoporosis: a review of the evidence and suggested guidelines for its use. Endocr Rev. Aug.2005 26:688–703. [PubMed: 15769903]
6. Tam CS, Heersche JN, Murray TM, Parsons JA. Parathyroid hormone stimulates the bone apposition rate independently of its resorptive action: differential effects of intermittent and continuous administration. Endocrinology. Feb.1982 110:506–512. [PubMed: 7056211]
7. Jilka RL. Molecular and cellular mechanisms of the anabolic effect of intermittent PTH. Bone. Jun. 2007 40:1434–1446. [PubMed: 17517365]
8. Qin L, Raggatt LJ, Partridge NC. Parathyroid hormone: a double-edged sword for bone metabolism. Trends Endocrinol Metab. Mar.2004 15:60–65. [PubMed: 15036251]
9. Tamai K, Semenov M, Kato Y, Spokony R, Liu C, Katsuyama Y, Hess F, Saint-Jeannet JP, He X. LDL-receptor-related proteins in Wnt signal transduction. Nature. Sep 28.2000 407:530–535. [PubMed: 11029007]
10. Pinson KI, Brennan J, Monkley S, Avery BJ, Skarnes WC. An LDL-receptor-related protein mediates Wnt signalling in mice. Nature. Sep 28.2000 407:535–538. [PubMed: 11029008]
11. Huelsken J, Birchmeier W. New aspects of Wnt signaling pathways in higher vertebrates. Curr Opin Genet Dev. Oct.2001 11:547–553. [PubMed: 11532397]
12. Mao J, Wang J, Liu B, Pan W, Farr GH III, Flynn C, Yuan H, Takada S, Kimelman D, Li L, Wu D. Low-density lipoprotein receptor-related protein-5 binds to Axin and regulates the canonical Wnt signaling pathway. Mol Cell. Apr.2001 7:801–809. [PubMed: 11336703]

13. Tamai K, Zeng X, Liu C, Zhang X, Harada Y, Chang Z, He X. A mechanism for Wnt coreceptor activation. Mol Cell. Jan 16.2004 13:149–156. [PubMed: 14731402]

14. Gong Y, Slee RB, Fukai N, Rawadi G, Roman-Roman S, Reginato AM, Wang H, Cundy T, Glorieux FH, Lev D, Zacharin M, Oexle K, Marcelino J, Suwairi W, Heeger S, Sabatakos G, Apte S, Adkins WN, Allgrove J, rslan-Kirchner M, Batch JA, Beighton P, Black GC, Boles RG, Boon LM, Borrone C, Brunner HG, Carle GF, Dallapiccola B, De PA, Floege B, Halfhide ML, Hall B, Hennekam RC, Hirose T, Jans A, Juppner H, Kim CA, Keppler-Noreuil K, Kohlschuetter A, LaCombe D, Lambert M, Lemyre E, Letteboer T, Peltonen L, Ramesar RS, Romanengo M, Somer H, Steichen-Gersdorf E, Steinmann B, Sullivan B, Superti-Furga A, Swoboda W, van den Boogaard MJ, Van HW, Vikkula M, Votruba M, Zabel B, Garcia T, Baron R, Olsen BR, Warman ML. LDL receptor-related protein 5 (LRP5) affects bone accrual and eye development. Cell. Nov 16.2001 107:513–523. [PubMed: 11719191]

15. Little RD, Recker RR, Johnson ML. High bone density due to a mutation in LDL-receptor-related protein 5. N Engl J Med. Sep 19.2002 347:943–944. [PubMed: 12239268]

16. Boyden LM, Mao J, Belsky J, Mitzner L, Farhi A, Mitnick MA, Wu D, Insogna K, Lifton RP. High bone density due to a mutation in LDL-receptor-related protein 5. N Engl J Med. May 16.2002 346:1513–1521. [PubMed: 12015390]

17. Little RD, Carulli JP, Del Mastro RG, Dupuis J, Osborne M, Folz C, Manning SP, Swain PM, Zhao SC, Eustace B, Lappe MM, Spitzer L, Zweier S, Braunschweiger K, Benchekroun Y, Hu X, Adair R, Chee L, FitzGerald MG, Tulig C, Caruso A, Tzellas N, Bawa A, Franklin B, McGuire S, Nogues X, Gong G, Allen KM, Anisowicz A, Morales AJ, Lomedico PT, Recker SM, Van EP, Recker RR, Johnson ML. A mutation in the LDL receptor-related protein 5 gene results in the autosomal dominant high-bone-mass trait. Am J Hum Genet. Jan.2002 70:11–19. [PubMed: 11741193]

18. Mani A, Radhakrishnan J, Wang H, Mani A, Mani MA, Nelson-Williams C, Carew KS, Mane S, Najmabadi H, Wu D, Lifton RP. LRP6 mutation in a family with early coronary disease and metabolic risk factors. Science. Mar 2.2007 315:1278–1282. [PubMed: 17332414]

19. van Meurs JB, Rivadeneira F, Jhamai M, Hugens W, Hofman A, van Leeuwen JP, Pols HA, Uitterlinden AG. Common genetic variation of the low-density lipoprotein receptor-related protein 5 and 6 genes determines fracture risk in elderly white men. J Bone Miner Res. Jan.2006 21:141–150. [PubMed: 16355283]

20. van Meurs JB, Trikalinos TA, Ralston SH, Balcells S, Brandi ML, Brixen K, Kiel DP, Langdahl BL, Lips P, Ljunggren O, Lorenc R, Obermayer-Pietsch B, Ohlsson C, Pettersson U, Reid DM, Rousseau F, Scollen S, Van HW, Agueda L, Akesson K, Benevolenskaya LI, Ferrari SL, Hallmans G, Hofman A, Husted LB, Kruk M, Kaptoge S, Karasik D, Karlsson MK, Lorentzon M, Masi L, McGuigan FE, Mellstrom D, Mosekilde L, Nogues X, Pols HA, Reeve J, Renner W, Rivadeneira F, van Schoor NM, Weber K, Ioannidis JP, Uitterlinden AG. Large-scale analysis of association between LRP5 and LRP6 variants and osteoporosis. JAMA. Mar 19.2008 299:1277–1290. [PubMed: 18349089]

21. Kato M, Patel MS, Levasseur R, Lobov I, Chang BH, Glass DA, Hartmann C, Li L, Hwang TH, Brayton CF, Lang RA, Karsenty G, Chan L. Cbfa1-independent decrease in osteoblast proliferation, osteopenia, and persistent embryonic eye vascularization in mice deficient in Lrp5, a Wnt coreceptor. J Cell Biol. Apr 15.2002 157:303–314. [PubMed: 11956231]

22. Kelly OG, Pinson KI, Skarnes WC. The Wnt co-receptors Lrp5 and Lrp6 are essential for gastrulation in mice. Development. Jun.2004 131:2803–2815. [PubMed: 15142971]

23. Holmen SL, Giambernardi TA, Zylstra CR, Buckner-Berghuis BD, Resau JH, Hess JF, Glatt V, Bouxsein ML, Ai M, Warman ML, Williams BO. Decreased BMD and limb deformities in mice carrying mutations in both Lrp5 and Lrp6. J Bone Miner Res. Dec.2004 19:2033–2040. [PubMed: 15537447]

24. Wan M, Yang C, Li J, Wu X, Yuan H, Ma H, He X, Nie S, Chang C, Cao X. Parathyroid hormone signaling through low-density lipoprotein-related protein 6. Genes Dev. Nov 1.2008 22:2968–2979. [PubMed: 18981475]

25. Qiu T, Wu X, Zhang F, Clemens TL, Wan M, Cao X. TGF-beta type II receptor phosphorylates PTH receptor to integrate bone remodelling signalling. Nat Cell Biol. Mar.2010 12:224–234. [PubMed: 20139972]

26. Yu B, Zhao X, Yang C, Crane J, Xian L, Lu W, Wan M, Cao X. Parathyroid hormone induces differentiation of mesenchymal stromal/stem cells by enhancing bone morphogenetic protein signaling. J Bone Miner Res. Sep.2012 27:2001–2014. [PubMed: 22589223]
27. Wan M, Li J, Herbst K, Zhang J, Yu B, Wu X, Qiu T, Lei W, Lindvall C, Williams BO, Ma H, Zhang F, Cao X. LRP6 mediates cAMP generation by G protein-coupled receptors through regulating the membrane targeting of Galpha(s). Sci Signal. 2011; 4:ra15. [PubMed: 21406690]
28. Sawakami K, Robling AG, Ai M, Pitner ND, Liu D, Warden SJ, Li J, Maye P, Rowe DW, Duncan RL, Warman ML, Turner CH. The Wnt co-receptor LRP5 is essential for skeletal mechanotransduction but not for the anabolic bone response to parathyroid hormone treatment. J Biol Chem. Aug 18.2006 281:23698–23711. [PubMed: 16790443]
29. Iwaniec UT, Wronski TJ, Liu J, Rivera MF, Arzaga RR, Hansen G, Brommage R. PTH stimulates bone formation in mice deficient in Lrp5. J Bone Miner Res. Mar.2007 22:394–402. [PubMed: 17147489]
30. Qin L, Qiu P, Wang L, Li X, Swarthout JT, Soteropoulos P, Tolias P, Partridge NC. Gene expression profiles and transcription factors involved in parathyroid hormone signaling in osteoblasts revealed by microarray and bioinformatics. J Biol Chem. May 30.2003 278:19723–19731. [PubMed: 12644456]
31. Lombardi G, Di SC, Rubino M, Faggiano A, Vuolo L, Guerra E, Contaldi P, Savastano S, Colao A. The roles of parathyroid hormone in bone remodeling: prospects for novel therapeutics. J Endocrinol Invest. Jul.2011 34:18–22. [PubMed: 21985975]
32. Zylstra CR, Wan C, VanKoevering KK, Sanders AK, Lindvall C, Clemens TL, Williams BO. Gene targeting approaches in mice: assessing the roles of LRP5 and LRP6 in osteoblasts. J Musculoskelet Neuronal Interact. Oct.2008 8:291–293. [PubMed: 19147944]
33. Joeng KS, Schumacher CA, Zylstra-Diegel CR, Long F, Williams BO. Lrp5 and Lrp6 redundantly control skeletal development in the mouse embryo. Dev Biol. Nov 15.2011 359:222–229. [PubMed: 21924256]
34. Zhang M, Xuan S, Bouxsein ML, von SD, Akeno N, Faugere MC, Malluche H, Zhao G, Rosen CJ, Efstratiadis A, Clemens TL. Osteoblast-specific knockout of the insulin-like growth factor (IGF) receptor gene reveals an essential role of IGF signaling in bone matrix mineralization. J Biol Chem. Nov 15.2002 277:44005–44012. [PubMed: 12215457]
35. Canalis E, Parker K, Feng JQ, Zanotti S. Osteoblast lineage-specific effects of notch activation in the skeleton. Endocrinology. Feb.2013 154:623–634. [PubMed: 23275471]
36. Jho EH, Zhang T, Domon C, Joo CK, Freund JN, Costantini F. Wnt/beta-catenin/Tcf signaling induces the transcription of Axin2, a negative regulator of the signaling pathway. Mol Cell Biol. Feb.2002 22:1172–1183. [PubMed: 11809808]
37. Leung JY, Kolligs FT, Wu R, Zhai Y, Kuick R, Hanash S, Cho KR, Fearon ER. Activation of AXIN2 expression by beta-catenin-T cell factor. A feedback repressor pathway regulating Wnt signaling. J Biol Chem. Jun 14.2002 277:21657–21665. [PubMed: 11940574]
38. Lustig B, Jerchow B, Sachs M, Weiler S, Pietsch T, Karsten U, van de Wetering M, Clevers H, Schlag PM, Birchmeier W, Behrens J. Negative feedback loop of Wnt signaling through upregulation of conductin/axin2 in colorectal and liver tumors. Mol Cell Biol. Feb.2002 22:1184–1193. [PubMed: 11809809]
39. Rousset R, Mack JA, Wharton KA Jr. Axelrod JD, Cadigan KM, Fish MP, Nusse R, Scott MP. Naked cuticle targets dishevelled to antagonize Wnt signal transduction. Genes Dev. Mar 15.2001 15:658–671. [PubMed: 11274052]
40. Waldrop S, Chan CC, Cagatay T, Zhang S, Rousset R, Mack J, Zeng W, Fish M, Zhang M, Amanai M, Wharton KA Jr. An unconventional nuclear localization motif is crucial for function of the Drosophila Wnt/wingless antagonist Naked cuticle. Genetics. Sep.2006 174:331–348. [PubMed: 16849595]
41. Kim JS, Crooks H, Dracheva T, Nishanian TG, Singh B, Jen J, Waldman T. Oncogenic beta-catenin is required for bone morphogenetic protein 4 expression in human cancer cells. Cancer Res. May 15.2002 62:2744–2748. [PubMed: 12019147]

42. Glass DA, Bialek P, Ahn JD, Starbuck M, Patel MS, Clevers H, Taketo MM, Long F, McMahon AP, Lang RA, Karsenty G. Canonical Wnt signaling in differentiated osteoblasts controls osteoclast differentiation. Dev Cell. May.2005 8:751–764. [PubMed: 15866165]
43. Holmen SL, Zylstra CR, Mukherjee A, Sigler RE, Faugere MC, Bouxsein ML, Deng L, Clemens TL, Williams BO. Essential role of beta-catenin in postnatal bone acquisition. J Biol Chem. Jun 3.2005 280:21162–21168. [PubMed: 15802266]
44. Baron R, Hesse E. Update on bone anabolics in osteoporosis treatment: rationale, current status, and perspectives. J Clin Endocrinol Metab. Feb.2012 97:311–325. [PubMed: 22238383]
45. Bellido T, Ali AA, Plotkin LI, Fu Q, Gubrij I, Roberson PK, Weinstein RS, O'Brien CA, Manolagas SC, Jilka RL. Proteasomal degradation of Runx2 shortens parathyroid hormone-induced anti-apoptotic signaling in osteoblasts. A putative explanation for why intermittent administration is needed for bone anabolism. J Biol Chem. Dec 12.2003 278:50259–50272. [PubMed: 14523023]
46. Chen HL, Demiralp B, Schneider A, Koh AJ, Silve C, Wang CY, McCauley LK. Parathyroid hormone and parathyroid hormone-related protein exert both pro- and anti-apoptotic effects in mesenchymal cells. J Biol Chem. May 31.2002 277:19374–19381. [PubMed: 11897779]
47. McCauley LK, Koh-Paige AJ, Chen H, Chen C, Ontiveros C, Irwin R, McCabe LR. Parathyroid hormone stimulates fra-2 expression in osteoblastic cells in vitro and in vivo. Endocrinology. May. 2001 142:1975–1981. [PubMed: 11316763]
48. Pearman AT, Chou WY, Bergman KD, Pulumati MR, Partridge NC. Parathyroid hormone induces c-fos promoter activity in osteoblastic cells through phosphorylated cAMP response element (CRE)-binding protein binding to the major CRE. J Biol Chem. Oct 11.1996 271:25715–25721. [PubMed: 8810350]
49. Tyson DR, Swarthout JT, Partridge NC. Increased osteoblastic c-fos expression by parathyroid hormone requires protein kinase A phosphorylation of the cyclic adenosine 3',5'-monophosphate response element-binding protein at serine 133. Endocrinology. Mar.1999 140:1255–1261. [PubMed: 10067851]
50. Selvamurugan N, Chou WY, Pearman AT, Pulumati MR, Partridge NC. Parathyroid hormone regulates the rat collagenase-3 promoter in osteoblastic cells through the cooperative interaction of the activator protein-1 site and the runt domain binding sequence. J Biol Chem. Apr 24.1998 273:10647–10657. [PubMed: 9553127]
51. Partridge NC, Walling HW, Bloch SR, Omura TH, Chan PT, Pearman AT, Chou WY. The regulation and regulatory role of collagenase in bone. Crit Rev Eukaryot Gene Expr. 1996; 6:15–27. [PubMed: 8882305]
52. Kramer I, Halleux C, Keller H, Pegurri M, Gooi JH, Weber PB, Feng JQ, Bonewald LF, Kneissel M. Osteocyte Wnt/beta-catenin signaling is required for normal bone homeostasis. Mol Cell Biol. Jun.2010 30:3071–3085. [PubMed: 20404086]
53. Fu Q, Jilka RL, Manolagas SC, O'Brien CA. Parathyroid hormone stimulates receptor activator of NFkappa B ligand and inhibits osteoprotegerin expression via protein kinase A activation of cAMP-response element-binding protein. J Biol Chem. Dec 13.2002 277:48868–48875. [PubMed: 12364326]
54. Fu Q, Manolagas SC, O'Brien CA. Parathyroid hormone controls receptor activator of NF-kappaB ligand gene expression via a distant transcriptional enhancer. Mol Cell Biol. Sep.2006 26:6453–6468. [PubMed: 16914731]
55. Kim S, Yamazaki M, Shevde NK, Pike JW. Transcriptional control of receptor activator of nuclear factor-kappaB ligand by the protein kinase A activator forskolin and the transmembrane glycoprotein 130-activating cytokine, oncostatin M, is exerted through multiple distal enhancers. Mol Endocrinol. Jan.2007 21:197–214. [PubMed: 17053039]
56. Swarthout JT, D'Alonzo RC, Selvamurugan N, Partridge NC. Parathyroid hormone-dependent signaling pathways regulating genes in bone cells. Gene. Jan 9.2002 282:1–17. [PubMed: 11814673]
57. Datta NS, Abou-Samra AB. PTH and PTHrP signaling in osteoblasts. Cell Signal. Aug.2009 21:1245–1254. [PubMed: 19249350]
58. Schipani E, Kronenberg HM. Adult mesenchymal stem cells. 2008

59. Ohishi M, Schipani E. PTH and stem cells. J Endocrinol Invest. Jul.2011 34:552–556. [PubMed: 21427529]

60. Mendez-Ferrer S, Michurina TV, Ferraro F, Mazloom AR, Macarthur BD, Lira SA, Scadden DT, Ma'ayan A, Enikolopov GN, Frenette PS. Mesenchymal and haematopoietic stem cells form a unique bone marrow niche. Nature. Aug 12.2010 466:829–834. [PubMed: 20703299]

61. Li JY, Adams J, Calvi LM, Lane TF, Dipaolo R, Weitzmann MN, Pacifici R. PTH expands short-term murine hemopoietic stem cells through T cells. Blood. Nov 22.2012 120:4352–4362. [PubMed: 22955916]

62. Calvi LM, Adams GB, Weibrecht KW, Weber JM, Olson DP, Knight MC, Martin RP, Schipani E, Divieti P, Bringhurst FR, Milner LA, Kronenberg HM, Scadden DT. Osteoblastic cells regulate the haematopoietic stem cell niche. Nature. Oct 23.2003 425:841–846. [PubMed: 14574413]

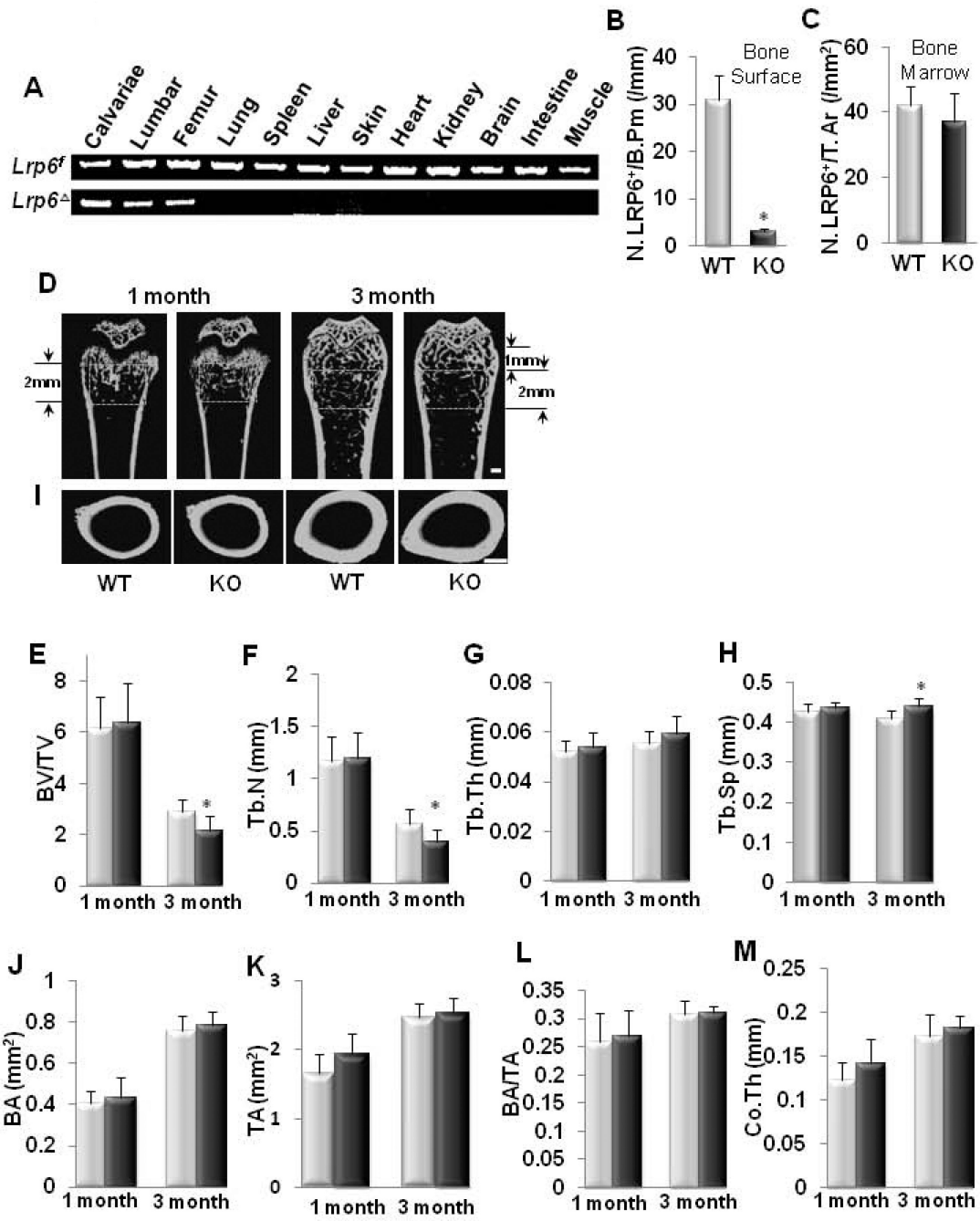

Fig. 1. Osteoblast-specific deletion of LRP6 causes bone loss in trabecular bone in adult but not in young mice

(**A**) PCR analysis was performed using different tissues harvested from LRP6 KO mice to examine specific deletion of *Lrp6*. Bands represent *Lrp6* gene alleles that are either flanked with a loxP site (*Lrp6*^{f}) or deleted (*Lrp*$^{\Delta}$). (**B** and **C**) Number of LRP6^{+} cells on bone surface (**B**) and in bone marrow (**C**). N. LRP6^{+} cells/B.Pm, number of LRP6-positive cells per bone perimeter. N. LRP6^{+} cells/T.Ar, number of LRP6-positive cells per tissue area. n = 7; *p < 0.001. Data are presented as mean ± SEM. (**D–H**) Representative μCT images and quantitative analysis of the trabecular bone area of distal femur from 1 and 3 month-old male mice. Yellow squares indicate the area chosen for analysis. Scale bar: 500μM.

Trabecular bone volume fraction (BV/TV) (**E**), trabecular number (Tb.N) (**F**), trabecular thickness (Tb.Th) (**G**), and trabecular separation (Tb. Sp) (**H**). Light blue column, WT; Dark blue column, KO. n = 10; *p < 0.05. (**I–M**) Representative μCT images and quantitative analysis of cross-sections of femoral mid-diaphyses from 1 and 3 month-old male mice. Scale bar: 500μM. Cortical bone area (BA) (**J**), total area with the periosteal circumference (TA) (**K**), cortical bone area as a percentage of total area within the periosteal circumference (BA/TA) (**L**), and cortical bone thickness (Co.Th) (**M**). n = 10. Light blue column, WT mice; Dark blue column, KO mice. Data are presented as mean ± SEM.

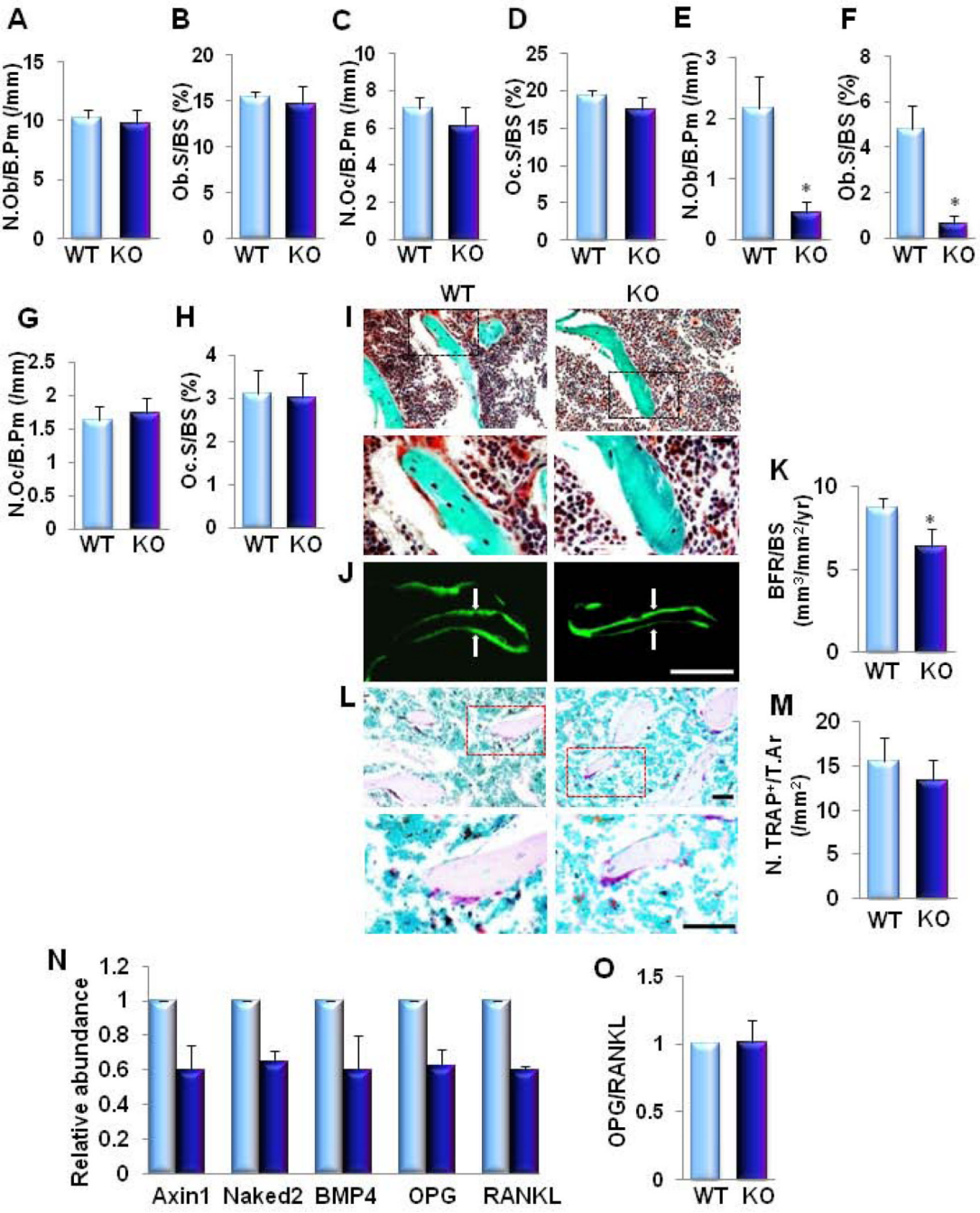

Fig. 2. Osteoblast-specific deletion of LRP6 causes decreased osteoblastic bone formation without affecting osteoclastic bone resorption in adult mice femora

(**A–D**) Bone histomorphometric analysis of trabecular bone from 1 month-old male mice. Number of osteoblasts per bone perimeter (N.Ob/B. Pm) (**A**), osteoblast surface per bone surface (Ob.S/BS) (**B**), number of osteoclasts per bone perimeter (N.Oc/B. Pm) (**C**), and osteoclast surface per bone surface (Oc.S/BS) (**D**). n = 8. (**E–H**) Bone histomorphometric analysis of trabecular bone of the secondary spongiosa from 3-month-old male mice. Number of osteoblasts per bone perimeter (N.Ob/ B. Pm) (**E**), osteoblast surface per bone surface (Ob.S/BS) (**F**), number of osteoclasts per bone perimeter (N.Oc/B. Pm) (**G**), and osteoclast surface per bone surface (Oc.S/BS) (**H**). n = 8. *p < 0.001. (**I**) Trichrome staining

of the metaphyseal trabecular bone at distal femora of 3 month-old mice. Mineralized bone stains green/blue and osteoid stains red. Upper panels are lower power image with boxes outlining the area of higher power in bottom panels. Scale bars: 100μM. (**J–K**) Representative calcein double labeling and quantification of bone formation rate of the metaphyseal trabecular bone at distal femora. Scale bar: 100μM (**J**). Bone formation rate per bone surface (BFR/BS (**K**)). n = 6. *p < 0.01. (**L–M**) Representative tartrate-resistant acid phophatase (TRAP) staining and quantitative analysis of trabecular bone sections from distal femur. Scale bars: 100μM (**L**). Number of TRAP-positive cells per mm^2 tissue area ($N.TRAP^+$ cells/T.Ar) (**M**). n = 7. (**N**) Quantitative RT-PCR analysis of β-catenin target genes (Axin2 , Naked2 , BMP4 , and OPG) and RANKL expression in bone tissue extracts from 3 month-old mice. Light blue column, WT; Dark blue column, KO. (**O**) Ratio of RANKL/OPG in bone tissue extracts from 3 month-old mice. n = 8; *p < 0.05. Data are presented as mean ± SEM.

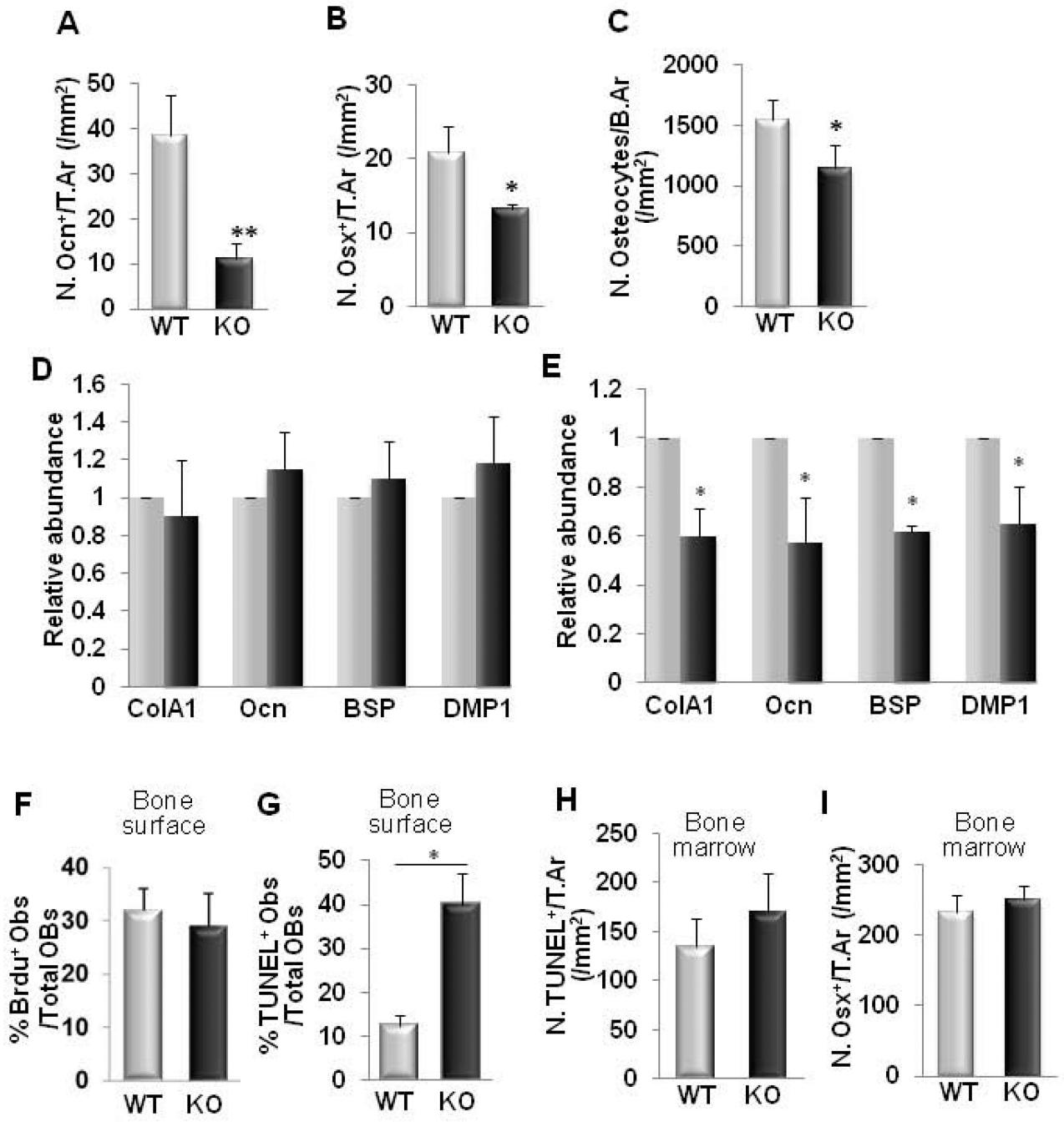

Fig. 3. LRP6-deficiency in osteoblasts leads to decreased expression of osteogenic genes and accelerated osteoblast apoptosis in femurs during bone remodeling

(**A–B**) Quantification of immunohistochemical staining for osteocalcin (Ocn) (**A**) and osterix (Osx) (**B**) in femur sections of 3 month-old male mice. Number of Ocn-positive cells per mm^2 tissue area ($N.Ocn^+$ cells/T.Ar), number of Osx-positive cells per mm^2 tissue area ($N.Osx^+$ cells/T.Ar). n = 8; *p < 0.01, **p < 0.001.. Data are presented as mean ± SEM. (**C**) Number of osteocytes in bone matrix. Number of osteocytes per mm^2 bone area (N.osteocytes/B.Ar), n = 8; *p < 0.05. (**D–E**) Quantitative RT-PCR analysis of osteoblast marker genes in bone tissue extract from 1 month- (**D**) and 3 month-old (**E**) WT and KO mice. Collagen 1A (Col1A), osteocalcin (Ocn), bone sialoprotein (BSP), dentin matrix

protein-1 (DMP1). n = 7; *p < 0.05. (**F**) Percentage of $BrdU^+$ osteoblasts out of total bone surface osteoblasts in the secondary spongiosa area in femur sections of 3-month-old mice. n = 8 (**G–H**) Analysis of apoptotic cells in trabecular bone (**G**) and bone marrow (**H**) of femur from 3 month-old WT and KO mice by TUNEL assay. Data presented as percentage of apoptotic osteoblasts out of total osteoblasts on bone surface (**G**) and number of TUNEL-positive cells per mm^2 tissue area ($N.TUNEL^+/T.Ar$) (**H**). n = 6. *p < 0.001. (**I**) Quantitative analysis of immunohistochemical staining for osterix (Osx) in secondary spongiosa bone marrow of femur sections in 3 month-old male mice. Number of Osx-positive cells per mm^2 tissue area ($N.Osx^+$ cells/T.Ar), n = 8; Data are presented as mean ± SEM.

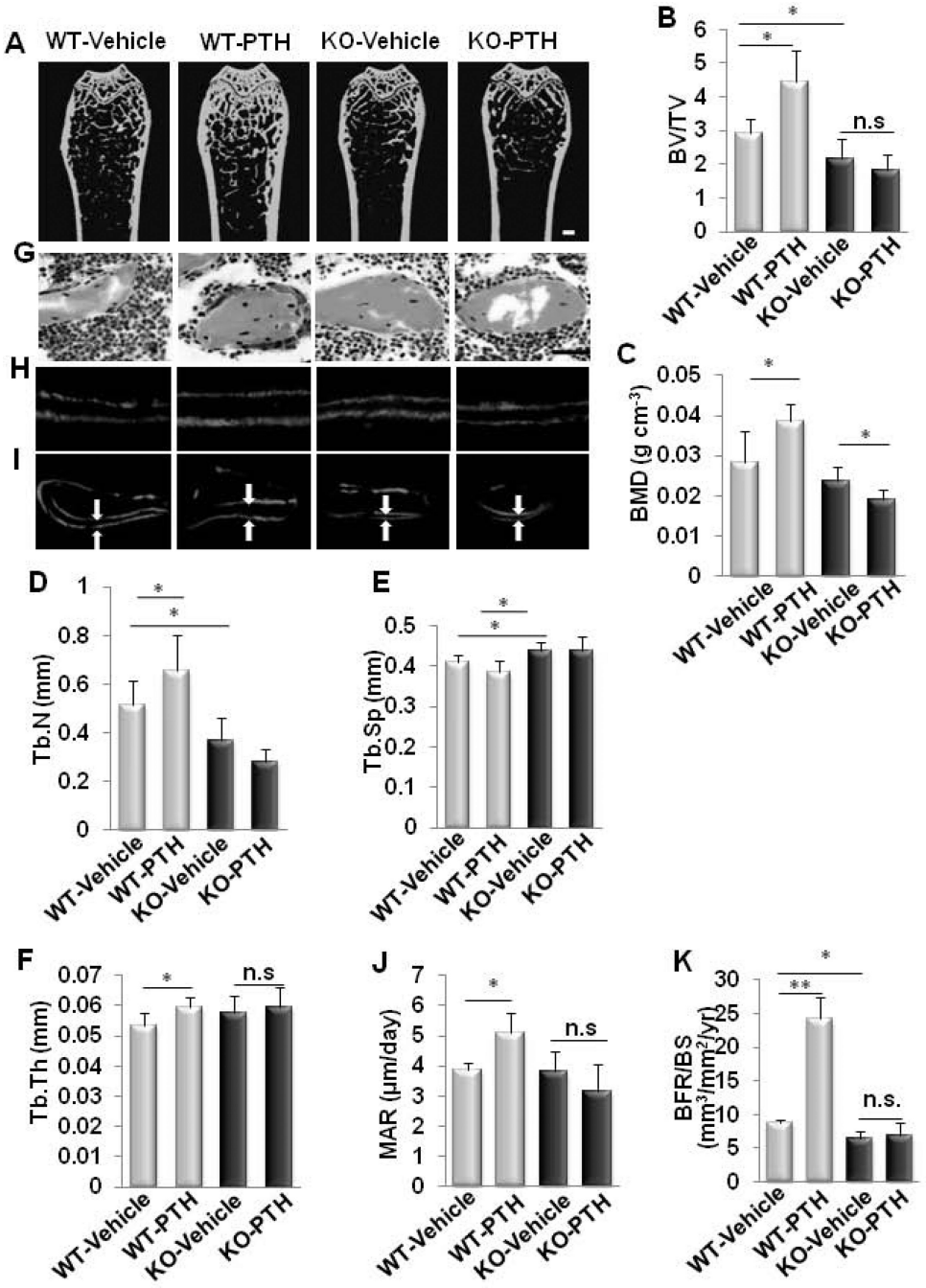

Fig. 4. Intermittent PTH treatment failed to increase bone formation in mice with osteoblast-specific deletion of *LRP6*

(**A–F**) Representative μCT images and quantitative analysis of distal femur from 3 month-old male mice treated with vehicle or PTH1–34 (80μg/kg. b.w, five days a week for four weeks). Scale bar: 500μM (**A**). Trabecular bone volume fraction (BV/TV) (**B**), bone mineral density (BMD) (**C**), trabecular number (Tb.N) (**D**), trabecular separation (Tb. Sp) (**E**), and trabecular thickness (Tb.Th) (**F**). n = 10 for each treatment group; *p < 0.05. **p < 0.01. (**G**) Trichrome staining of metaphyseal trabecular bone at distal femora from 3 month-old male mice treated with vehicle or PTH1–34 (80μg/kg. b.w, five days a week for four weeks). Mineralized bone stains green/blue and osteoid that lines bone stains red. Scale bar: 100μM.

(**H** and **I**) Calcein double labeling of cortical (**H**) and metaphyseal trabecular bone (**I**) in distal femora. Scale bars: 10μM for (**H**), and 100μM for (**I**). (**J–K**) Mineral apposition rate (MAR) (**J**) and bone formation rate per bone surface (BFR/BS) (**K**). n = 6; *p < 0.05, **p < 0.001. (**L–M**) Serum levels of osteocalcin (Ocn) (**L**) and c-terminal telopeptide of type-1 collagen (CTX-I) (**M**) in vehicle- or PTH-treated WT and KO mice. n = 7; *p < 0.001. Data are presented as mean ± SEM.

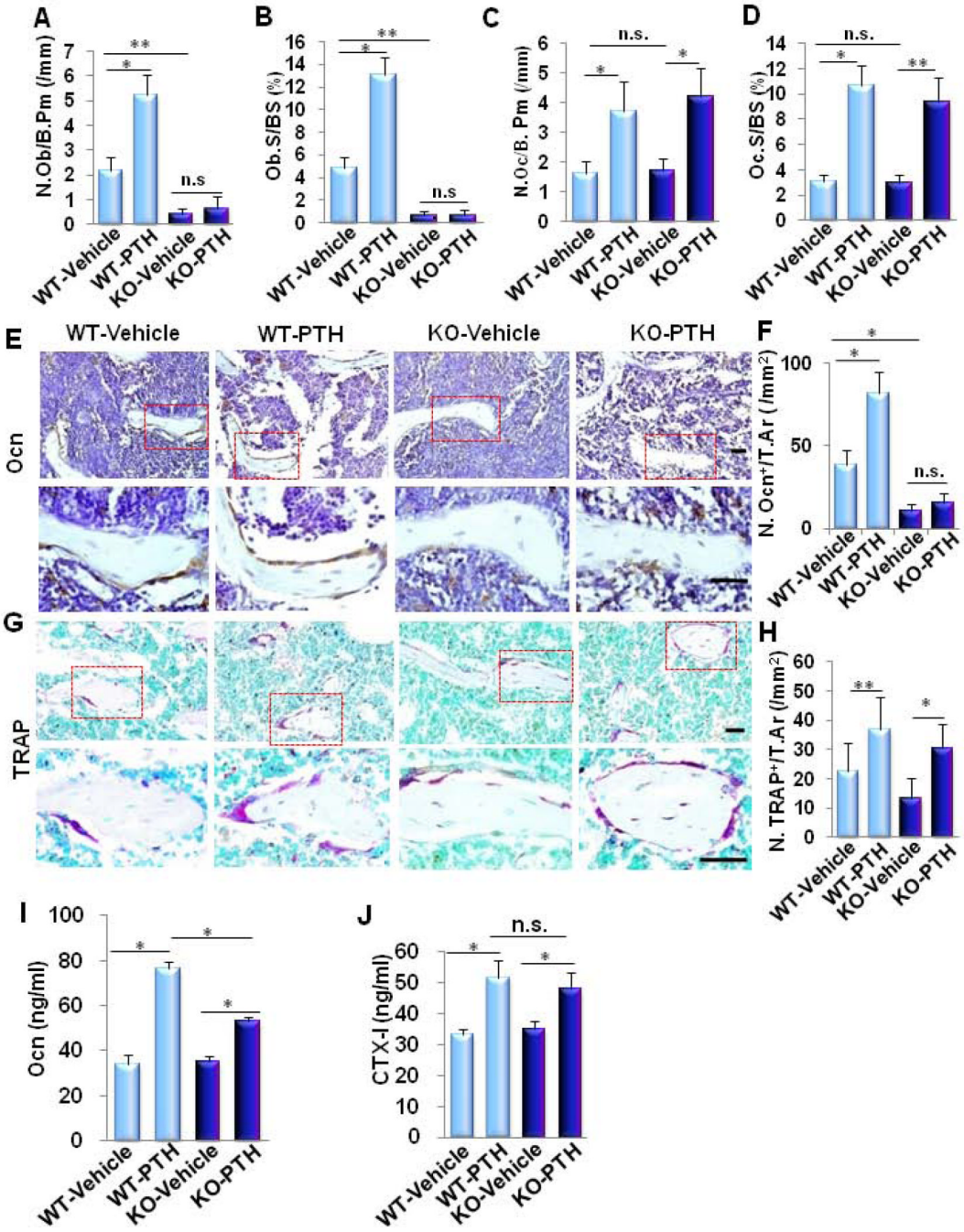

Fig. 5. LRP6 in osteoblasts is essential for PTH-stimulated osteoblastic bone formation but not osteoclastic bone resorption

(**A–D**) Bone histomorphometric analysis of trabecular bone in the secondary spongiosa of 3-month-old male mice treated with vehicle or PTH1–34 (80μg/kg. b.w, five days a week for four weeks). Number of osteoblasts per bone surface (N.Ob/B. Pm) (**A**), osteoblast surface per bone surface (Ob.S/BS) (**B**), number of osteoclasts per bone surface (N.Oc/ B. Pm) (**C**), and osteoclast surface per bone surface (Oc.S/BS) (**D**). n = 8; *p < 0.001. (**E–H**) Representative immunohistochemical staining and quantitative analysis of osteocalcin (Ocn) (**E–F**) and tartrate resistant acid phosphatase (TRAP) (**H-I**) in femur sections of 3 month-old male mice treated with vehicle or PTH(1–34) (80μg/kg. b.w, five days a week for four

weeks). Scale bars: 100μM (**E and H**). Number of osteocalcin-positive cells per mm^2 tissue area ($N.Ocn^+$ cells/T.Ar.) (**F**), number of TRAP-positive cells per mm^2 tissue area ($N.TRAP^+$ cells/T.Ar.) (**H**). n = 7; **p < 0.05, *p < 0.001. (**I**-**J**) Serum levels of osteocalcin (Ocn) (**I**) and c-terminal telopeptide of type-1 collagen (CTX-I) (**J**) in vehicle- or PTH-treated WT and KO mice. n = 7; *p < 0.001. Data are presented as mean ± SEM.

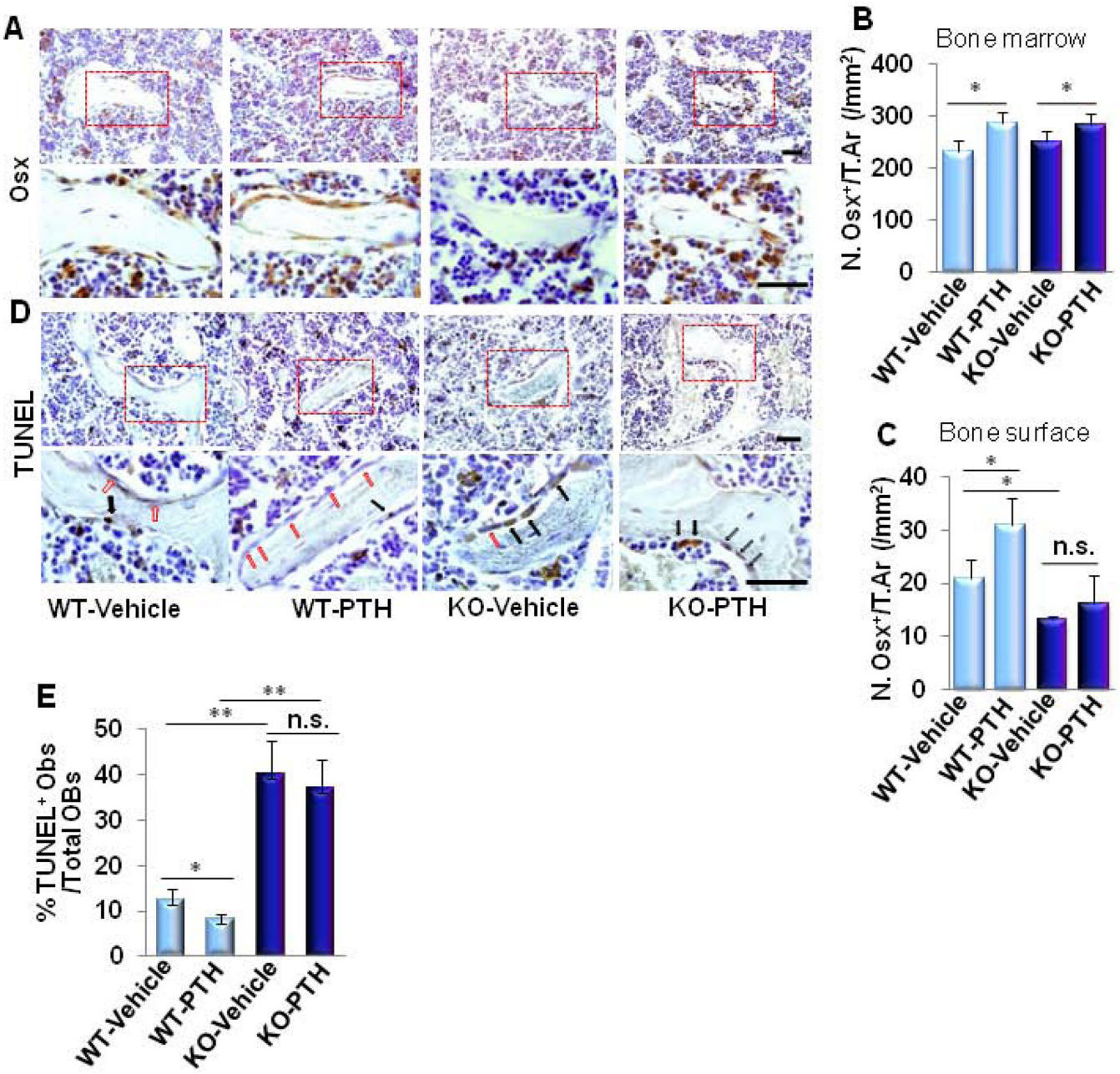

Fig. 6. LRP6 deficiency in osteoblasts impairs PTH-stimulated anti-apoptotic effects on osteoblasts without affecting PTH-increased bone marrow osteoprogenitors

(**A–C**) Representative immunohistochemical staining and quantitative analysis of osterix (Osx) in femur sections of 3 month-old male mice treated with vehicle or PTH1–34 (80μg/kg. b.w, five days a week for four weeks). Scale bars: 100μM (**A**). Number of Osx-positive cells per mm^2 tissue area. ($N.Osx^+$ cells/T.Ar) in bone marrow (**B**) and on bone surface (**C**). (**D–E**) Representative immunohistochemical staining and quantitative analysis of $TUNEL^+$ cells in femur sections of 3 month-old male mice treated with vehicle or PTH1–34 (80μg/kg. b.w, five days a week for four weeks). Black arrow: $TUNEL^+$ osteoblasts, red arrow: TUNEL osteoblasts. Scale bars: 100μM (**D**). Percentage of $TUNEL^+$ osteoblasts out of the total osteoblasts on bone surface (**E**). Red boxes in upper panels of A and D represent higher

magnification shown in lower panels, respectively. n = 7 for each treatment group; *p < 0.05, **p < 0.001. Data are presented as mean ± SEM.

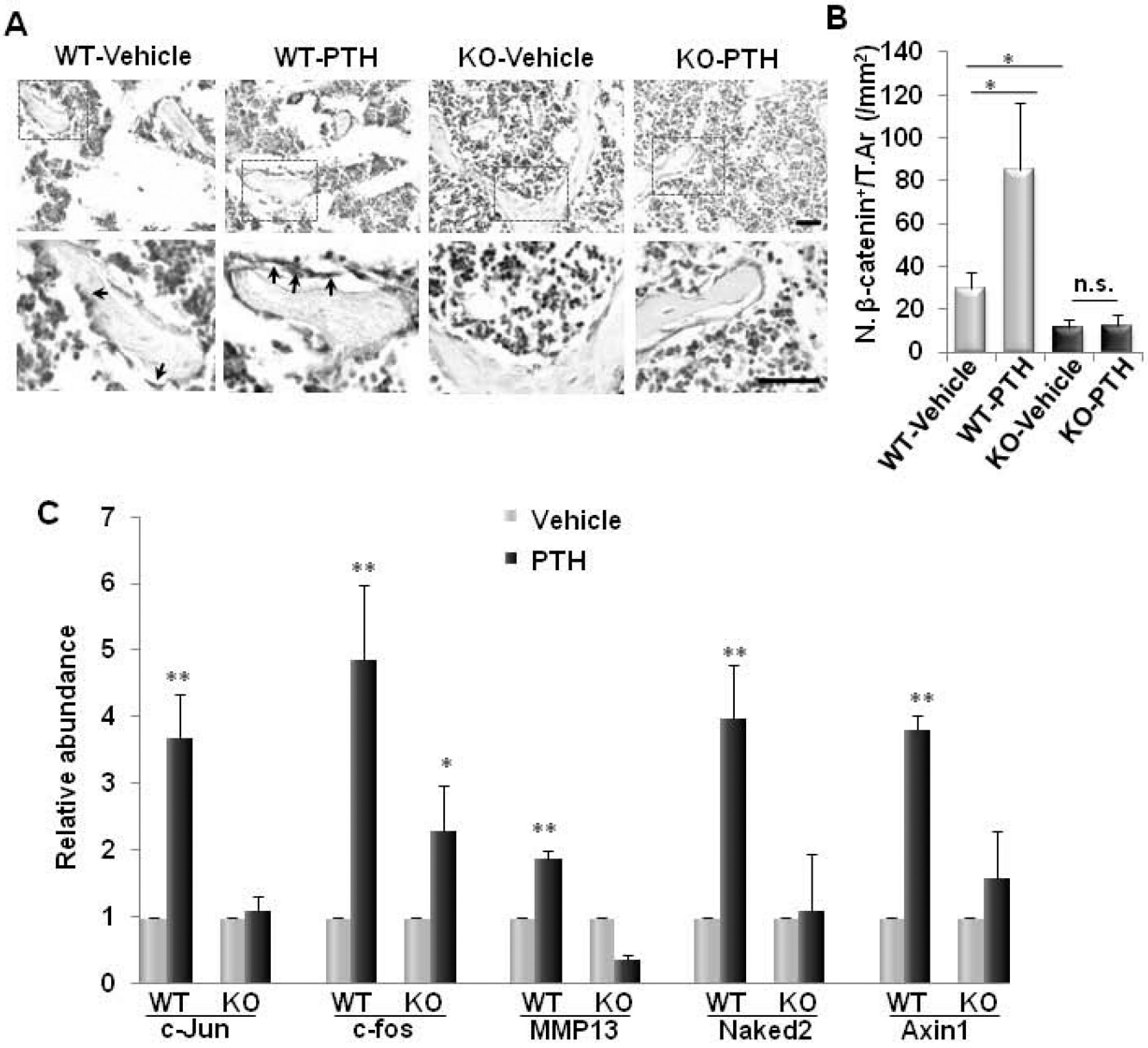

Fig. 7. PTH failed to stimulate β-catenin and $G\alpha_s$-PKA signaling in LRP6-deficient osteoblasts

(**A**–**B**) Representative immunohistochemical staining and quantitative analysis of β-catenin in femur sections of 3 month-old male mice treated with vehicle or PTH1–34 (80μg/kg. b.w, five days a week for four weeks). Arrows indicate β-catenin$^+$ osteoblasts on bone surface. Scale bars: 100μM (**A**). Number of β-catenin-positive cells per mm^2 tissue area (N. β-catenin$^+$ cells/T.Ar) (**B**). n = 7 for each treatment group; *p < 0.001. (**C**) Quantitative RT-PCR analysis of $G\alpha_s$-PKA target genes (c-JUN, c-Fos, and MMP13) and β-catenin target genes (Naked2 and Axin2) in calvarial osteoblasts isolated from *Lrp6$^{f/f}$* mice infected with adenovirus carrying either GFP (WT) or Cre (KO). Cells were treated with osteogenic medium in combination with either vehicle or PTH. n = 8; *p < 0.05. Data are presented as mean ±SEM.

Table 1

Baseline skeletal phenotype in 1 month-old and 3 month-old mice

Values presented are mean±SEM

1 month-old mice	**Male**			**Female**		
	WT (n=10)	**KO (n=10)**	***P value***	**WT (n=10)**	**KO (n=10)**	***P value***
Femoral length (mm)	13.41±0.90	13.79±0.99	*0.34*	11.56±0.84	11.89±0.88	*0.48*
Body mass (g)	18.24±3.33	20.24±3.27	*0.15*	14.58±1.68	15.39±2.28	*0.41*
3 month-old mice	Male			Female		
	WT (n=10)	KO (n=10)	*P value*	WT (n=10)	KO (n=10)	*P value*
Femoral length (mm)	15.95±0.75	15.62±0.75	*0.5*	14.80±0.28	15.00±0.50	*0.50*
Body mass (g)	28.32±1.77	29.83±1.96	*0.25*	19.60±1.82	20.20±0.97	*0.61*

J Bone Miner Res. Author manuscript; available in PMC 2014 October 01.